CHAPTER 5

THE DEAD-BAND CONTROL STRATEGY

5.1 Introduction

As discussed in the previous chapter, the strategy of adopting maximum constant D_0 control renders the capacitor voltage decreasing to a much lower level without influencing the high performance of the active rectifier. In this chapter, it is desired to enhance the rectifier efficiency further by reducing the switching number of the active switches. In fact, it is possible to reduce the switching number by one sixth during each interval of the AC voltage source for each phase. Although it is required to take some effort to distinguish the proper intervals for this new control strategy, however, an additional advantage, namely to achieve an even lower V_C voltage, can be obtained. Detailed theoretical basis of the proposed discontinuous duty ratio function strategy will be given in the following sections.

5.2 The Proposed Dead-Band Control

The dead-band control concept has been applied to a three-phase boost rectifier [10] to reduce the switching number successfully. From the Kirchhoff's current law, the sum of three line currents equals to zero. Hence, for each 60^0 of the AC source

period, one can fix the active switch status for the bridge arm whose current magnitude is at maximum among three phases. The four switches in the remaining two bridge arms are then modulated to control the two line currents to track the desired waveforms. Thus, no switching actions is made for the line current with maximum current magnitude during this period. This will not only reduce the switching loss but also will reduce the corresponding on/off electrical stress.

A similar concept is now applied to the proposed boostbuck rectifier. For convenient reference, the following modulating functions will be repeated:

$$\frac{m_1(t)}{2} = \frac{1}{v_C}(e_a - R_S i_a - L_S \frac{di_a}{dt}) \equiv d_m \cos(\omega t - \phi) \tag{5.1}$$

$$\frac{m_2(t)}{2} = \frac{1}{v_C}(e_b - R_S i_b - L_S \frac{di_b}{dt}) \equiv d_m \cos(\omega t - \phi - 120^0) \tag{5.2}$$

$$\frac{m_3(t)}{2} = \frac{1}{v_C}(e_c - R_S i_c - L_S \frac{di_c}{dt}) \equiv d_m \cos(\omega t - \phi + 120^0) \tag{5.3}$$

Instead of dividing the AC source period according to the a-phase current function, the six intervals, namely A, B, C, D, E, F, are divided by using $\frac{m_1(t)}{2}$ as the reference. Table 5.1 summarizes the precise definition of these intervals. As an illustration of the proposed strategy, first consider interval A. During this interval, one can see that $\frac{m_1(t)}{2}$ has the maximum magnitude among three modulation functions. In fact, one has the following inequality

$$d_1(t) > d_2(t) > d_3(t) \tag{5.4}$$

Since

$$d_1(t) = \frac{1+d_0}{2} + \frac{m_1(t)}{2} = \frac{1+d_0}{2} + d_m \cos(\omega t - \phi) \qquad (5.5)$$

$$d_2(t) = \frac{1+d_0}{2} + \frac{m_2(t)}{2} = \frac{1+d_0}{2} + d_m \cos(\omega t - \phi - 120^0) \qquad (5.6)$$

$$d_3(t) = \frac{1+d_0}{2} + \frac{m_3(t)}{2} = \frac{1+d_0}{2} + d_m \cos(\omega t - \phi + 120^0), \qquad (5.7)$$

from the dead-band control concept one can choose

$$d_1(t) = 1, \quad \forall\, t \in A \qquad (5.8)$$

Table 5.1 Precise definition of the six intervals

Interval	Range
Interval A	$\phi \le \omega t < \phi + \frac{\pi}{3}$
Interval B	$\phi + \frac{\pi}{3} \le \omega t < \phi + \frac{2\pi}{3}$
Interval C	$\phi + \frac{2\pi}{3} \le \omega t < \phi + \pi$
Interval D	$\phi + \pi \le \omega t < \phi + \frac{4\pi}{3}$
Interval E	$\phi + \frac{4\pi}{3} \le \omega t < \phi + \frac{5\pi}{3}$
Interval F	$\phi + \frac{5\pi}{3} \le \omega t < \phi + 2\pi$

It follows from equations (5.5) to (5.8) that

$$\frac{1+d_0}{2} = 1 - \frac{m_1(t)}{2} \tag{5.9}$$

$$d_2(t) = 1 - \frac{m_1(t)}{2} + \frac{m_2(t)}{2} \tag{5.10}$$

$$d_3(t) = 1 - \frac{m_1(t)}{2} + \frac{m_3(t)}{2} \tag{5.11}$$

$$= 1 - \sqrt{3} d_m \cos(\omega t - \varphi - 60^0)$$

Thus, from the maximum D_0 control strategy of the previous chapter, one can choose minimum $d_3(t)$ as the desired maximum constant duty ratio, D_0, as follows:

$$\begin{aligned} D_0 &= \min_t (d_3(t)) \\ &= 1 - \sqrt{3} d_m \ , \quad \forall t \in A \end{aligned} \tag{5.12}$$

It is worth pointing out that from equation (5.11) one can see

$$1 - \sqrt{3} d_m \le d_3(t) \le 1 - \frac{\sqrt{3}}{2} d_m \tag{5.13}$$

During this interval, one has only V_{70} vector and no V_{07} vector is available. Hence, the maximum constant D_0 is chosen to be $1 - \sqrt{3} d_m$. As a result, a typical duty ratio control pattern during this interval is shown in Fig. 5.1 where

$$\begin{aligned} d_1(t) &= 1 \\ d_2(t) &= 1 - \frac{m_1(t)}{2} + \frac{m_2(t)}{2} \\ d_3(t) &= 1 - \frac{m_1(t)}{2} + \frac{m_3(t)}{2} \\ d_4(t) &= D_0 = 1 - \sqrt{3} d_m \\ d_5(t) &= D_0 + \frac{m_1(t)}{2} - \frac{m_2(t)}{2} \\ d_6(t) &= D_0 + \frac{m_1(t)}{2} - \frac{m_3(t)}{2} \\ d_7(t) &= 1 - D_0 \end{aligned} \tag{5.14}$$

From Fig. 5.1, one can see for integrating the energy transfer from the AC side to the DC side, V_{77} vector is applied for a constant time interval, namely $D_0 T_S$. The constant D_0 control simplifies the implementation greatly and the realization technique of the previous chapter can be applied to this control strategy too. As another illustration, consider the next time interval, namely B of Table 5.1. It is seen during this interval that

$$d_2(t) > d_1(t) > d_3(t). \tag{5.15}$$

From symmetrical consideration, for the lower bridge arms

$$d_6(t) > d_4(t) > d_5(t) \tag{5.16}$$

Thus, one can choose

$$d_6(t) = \frac{1+d_0}{2} - \frac{m_3(t)}{2} = 1, \ \forall t \in B \tag{5.17}$$

It follows from equation (5.17) that

$$\frac{1+d_0}{2} = 1 + \frac{m_3(t)}{2} \tag{5.18}$$

$$d_4(t) = 1 - \frac{m_1(t)}{2} + \frac{m_3(t)}{2} \tag{5.19}$$

$$d_5(t) = 1 - \frac{m_2(t)}{2} + \frac{m_3(t)}{2} \tag{5.20}$$

$$= 1 - \sqrt{3} d_m \cos(\omega t - \varphi - 90^0)$$

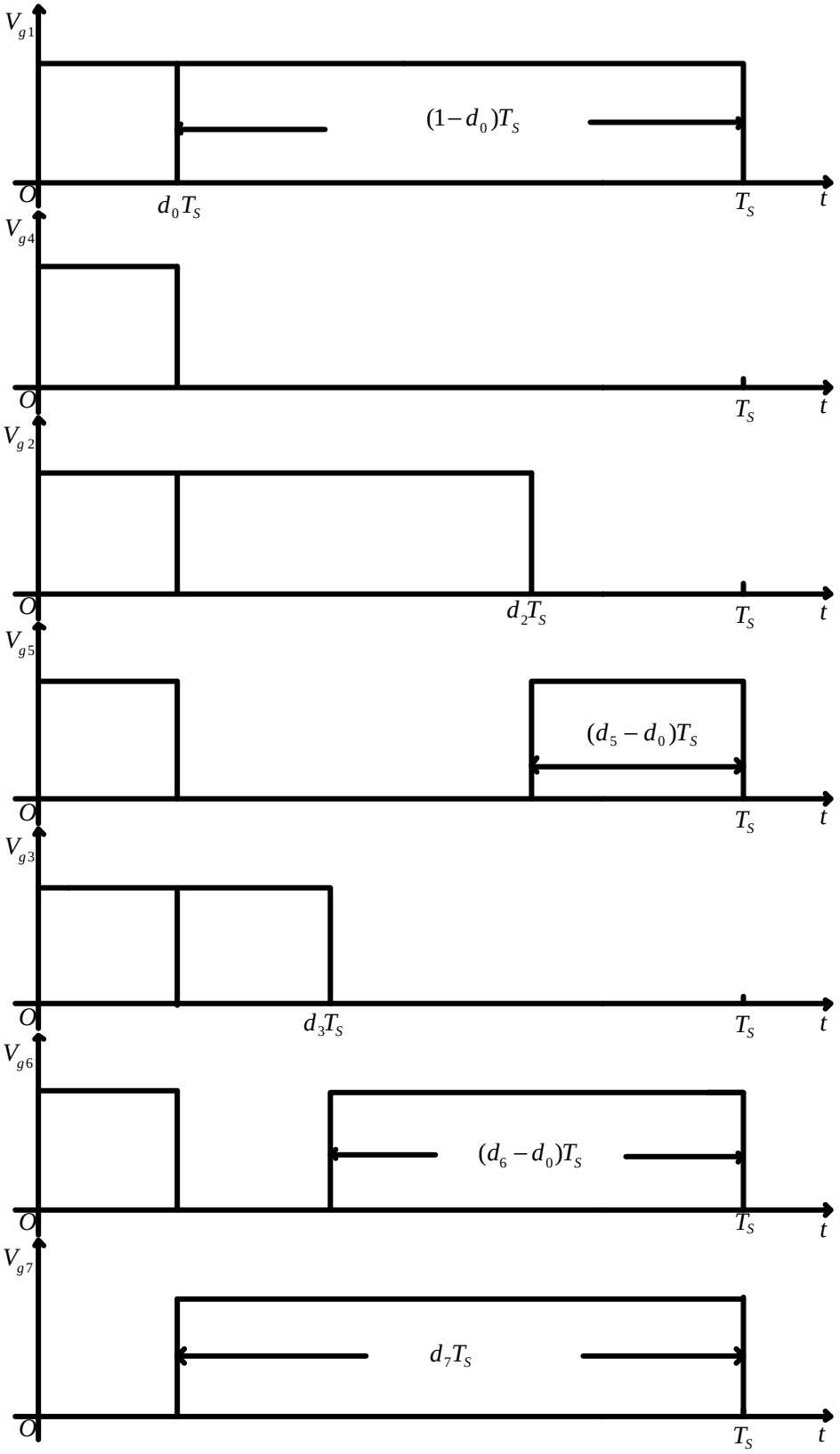

Fig. 5.1 A typical discontinuous duty ratio control pattern for $t \in A$

Thus, from the maximum constant D_0 control strategy, one can choose maximum d_0 as follows:

$$\begin{aligned} D_0 &= \underset{t}{Min}\ (d_5(t)) \\ &= 1-\sqrt{3}d_m\ , \quad \forall t \in B \end{aligned} \tag{5.21}$$

Fig. 5.2 shows a typical duty ratio function pattern as an illustration of how the V_{77} is added. It is seen from equation (5.21) that the chosen maximum constant d_0 is identical to that chosen in interval A. In fact, after proceeding the similar process for other intervals, the same conclusion is still valid. Table 5.2 summarizes the closed form duty ratio functions for different time intervals. Compared with the result of the previous chapter, one can see that the maximum D_0 for the dead-band case, namely $1-\sqrt{3}d_m$, is greater than that of the previous chapter, namely $1-2d_m$. In other words, the capacitor voltage, V_C, can be lower and with the merit of reducing switching loss and stress.

5.3 The Proposed Controller

Before presenting the proposed controller, one can observe first the regularity of the closed form duty ratio functions of the proposed control strategy as shown in Table 5.2. Hence, first define the following binary-value function $z(x)$:

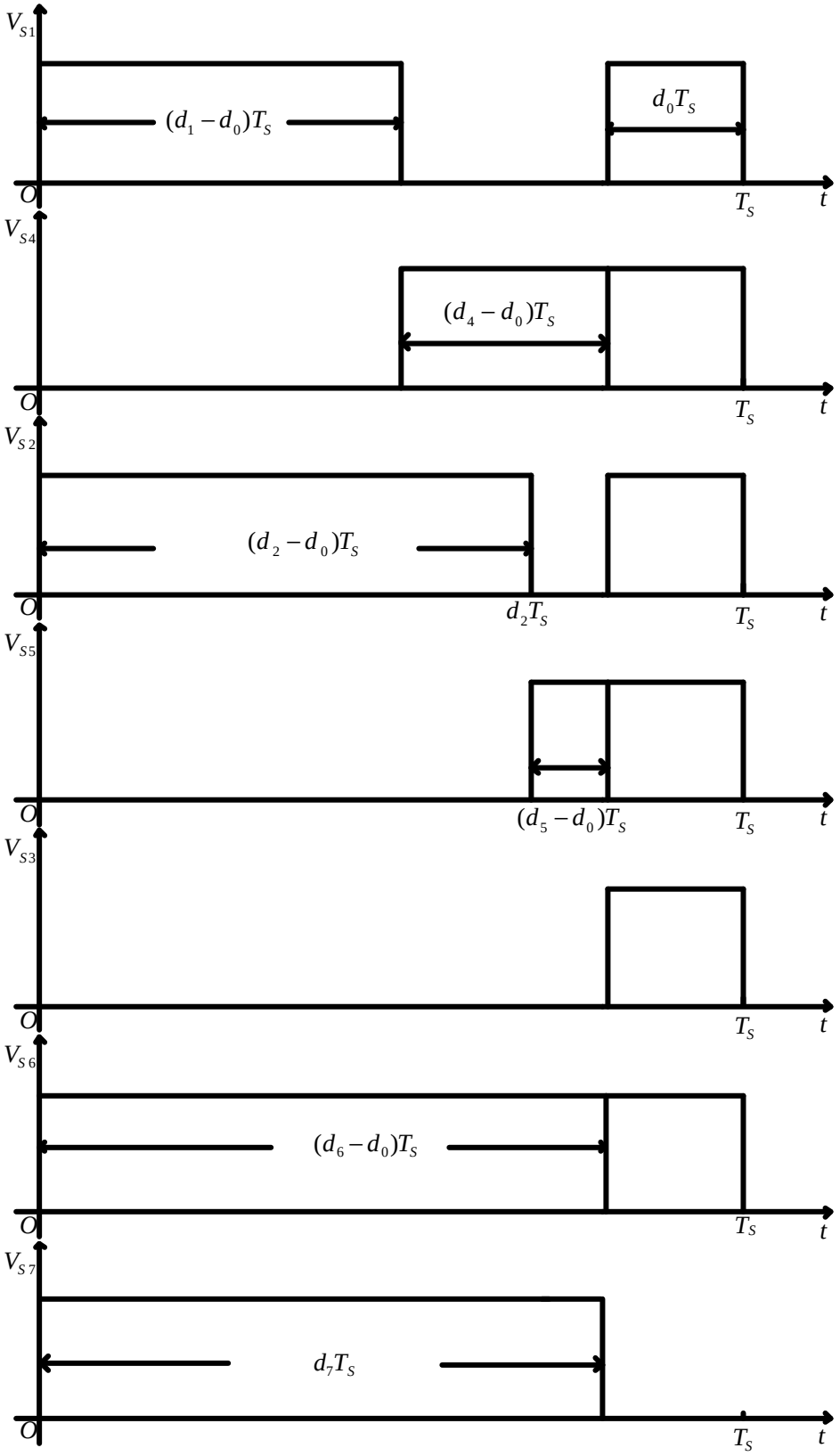

Fig. 5.2 A typical discontinuous duty ratio control pattern for $t \in B$

Table 5.2 Closed form duty ratio functions of the dead-band control strategy

Interval / duty ratio	A	B	C	D	E	F
d_1	1	$D_0+\frac{m_1(t)}{2}-\frac{m_3(t)}{2}$	$1-\frac{m_2(t)}{2}+\frac{m_1(t)}{2}$	D_0	$1-\frac{m_3(t)}{2}+\frac{m_1(t)}{2}$	$D_0+\frac{m_1(t)}{2}-\frac{m_2(t)}{2}$
d_2	$1-\frac{m_1(t)}{2}+\frac{m_2(t)}{2}$	$D_0+\frac{m_2(t)}{2}-\frac{m_3(t)}{2}$	1	$D_0+\frac{m_2(t)}{2}-\frac{m_1(t)}{2}$	$1-\frac{m_3(t)}{2}+\frac{m_2(t)}{2}$	D_0
d_3	$1-\frac{m_1(t)}{2}+\frac{m_3(t)}{2}$	D_0	$1-\frac{m_2(t)}{2}+\frac{m_3(t)}{2}$	$D_0+\frac{m_3(t)}{2}-\frac{m_1(t)}{2}$	1	$D_0+\frac{m_3(t)}{2}-\frac{m_2(t)}{2}$
d_4	D_0	$1-\frac{m_1(t)}{2}+\frac{m_3(t)}{2}$	$D_0+\frac{m_2(t)}{2}-\frac{m_1(t)}{2}$	1	$D_0+\frac{m_3(t)}{2}-\frac{m_1(t)}{2}$	$1-\frac{m_1(t)}{2}+\frac{m_2(t)}{2}$
d_5	$D_0+\frac{m_1(t)}{2}-\frac{m_2(t)}{2}$	$1-\frac{m_2(t)}{2}+\frac{m_3(t)}{2}$	D_0	$1-\frac{m_2(t)}{2}+\frac{m_1(t)}{2}$	$D_0+\frac{m_3(t)}{2}-\frac{m_2(t)}{2}$	1
d_6	$D_0+\frac{m_1(t)}{2}-\frac{m_3(t)}{2}$	1	$D_0+\frac{m_2(t)}{2}-\frac{m_3(t)}{2}$	$1-\frac{m_3(t)}{2}+\frac{m_1(t)}{2}$	D_0	$1-\frac{m_3(t)}{2}+\frac{m_2(t)}{2}$
d_7	$1-D_0$	$1-D_0$	$1-D_0$	$1-D_0$	$1-D_0$	$1-D_0$

$$z(x) = \begin{cases} 1 & , \quad \forall\, t \in x \\ 0 & , \quad \text{otherwise} \end{cases} \tag{5.22}$$

where

$$x \in \{A, B, C, D, E, F\} \tag{5.23}$$

Then, applying the same implementation technique as used in the previous chapter,

one can calculate

$$\frac{m_1(t)}{2} = \frac{1}{v_C}[e_a(t) - R_S I_m \cos(\omega t - \phi) + \omega L_S I_m \sin(\omega t - \phi)] \tag{5.24}$$

$$\frac{m_2(t)}{2} = \frac{1}{v_C}[e_b(t) - R_S I_m \cos(\omega t - \phi - 120^0) + \omega L_S I_m \sin(\omega t - \phi - 120^0)] \tag{5.25}$$

$$\frac{m_3(t)}{2} = \frac{1}{v_C}[e_c(t) - R_S I_m \cos(\omega t - \phi + 120^0) + \omega L_S I_m \sin(\omega t - \phi + 120^0)], \tag{5.26}$$

and similarly define the following duty ratio functions for the dead-band case

$$\begin{aligned} d_{az}(t) = {} & z(A)\cdot 1 + z(B)\cdot\left(\frac{m_1}{2} - \frac{m_3}{2}\right) + z(C)\cdot\left(1 - \frac{m_2}{2} + \frac{m_1}{2}\right) \\ & + z(D)\cdot 0 + z(E)\cdot\left(1 - \frac{m_3}{2} + \frac{m_1}{2}\right) + z(F)\cdot\left(\frac{m_1}{2} - \frac{m_2}{2}\right) \end{aligned} \tag{5.27}$$

$$\begin{aligned} d_{bz}(t) = {} & z(A)\cdot\left(1 - \frac{m_1}{2} + \frac{m_2}{2}\right) + z(B)\cdot\left(\frac{m_2}{2} - \frac{m_3}{2}\right) + z(C)\cdot 1 \\ & + z(D)\cdot\left(\frac{m_2}{2} - \frac{m_1}{2}\right) + z(E)\cdot\left(1 - \frac{m_3}{2} + \frac{m_2}{2}\right) + z(F)\cdot 0 \end{aligned} \tag{5.28}$$

$$\begin{aligned} d_{cz}(t) = {} & z(A)\cdot\left(1 - \frac{m_1}{2} + \frac{m_3}{2}\right) + z(B)\cdot 0 + z(C)\cdot\left(1 - \frac{m_2}{2} + \frac{m_3}{2}\right) \\ & + z(D)\cdot\left(\frac{m_3}{2} - \frac{m_1}{2}\right) + z(E)\cdot 1 + z(F)\cdot\left(\frac{m_3}{2} - \frac{m_2}{2}\right) \end{aligned} \tag{5.29}$$

Thus, by comparing d_{az}, d_{bz} and d_{cz} with the triangular waveform one can obtain the desired gating signals of S_1, S_2 and S_3, respectively. However, as in the

previous chapter, to achieve maximum constant D_0 control, one must add extra turn-on time period, namely D_0T_S, to S_1, S_2 and S_3 for $t \in x$ and $x \in \{B, D, F\}$ as shown in Fig. 5.2 for the case $t \in B$. In other words, during period D_0T_S, V_{77} is applied to transfer the energy from V_C to the output. Fig. 5.3 shows an implementation block diagram of the first switch signal generator. From Fig. 5.3 one can see that $t \in x$ and $x \in \{A, C, E\}$, $z(A) + z(B) + z(C) = 0$ and no extra turn-on time period is added to S_1, S_2 and S_3. Similarly, Fig. 5.4 shows an implementation block diagram of the second switch signal generator for S_4, S_5 and S_6. From Fig. 5.4 one can see that extra D_0T_S is added to S_4, S_5 and S_6 for transferring the energy from V_C to the output when $t \in x$ and $x \in \{A, C, E\}$. For $t \in x$ and $x \in \{B, D, F\}$ again no extra turn-on time period is added to S_4, S_5 and S_6.

Finally, whenever there is no energy transfer from V_C to the output, or equivalently whenever V_{77} is not applied, then S_7 is turned on. Fig. 5.5 shows a complete schematic block diagram of the proposed controller. From Fig. 5.5 one can see that a PI output voltage feedback control is used to generate the desired I_m command. Also a section detector is used to distinguish which time interval of $\{A, B, C, D, E, F\}$ is located. The magnitude d_m is obtained through a peak detector. In addition, the maximum D_0 is obtained through closed loop control as

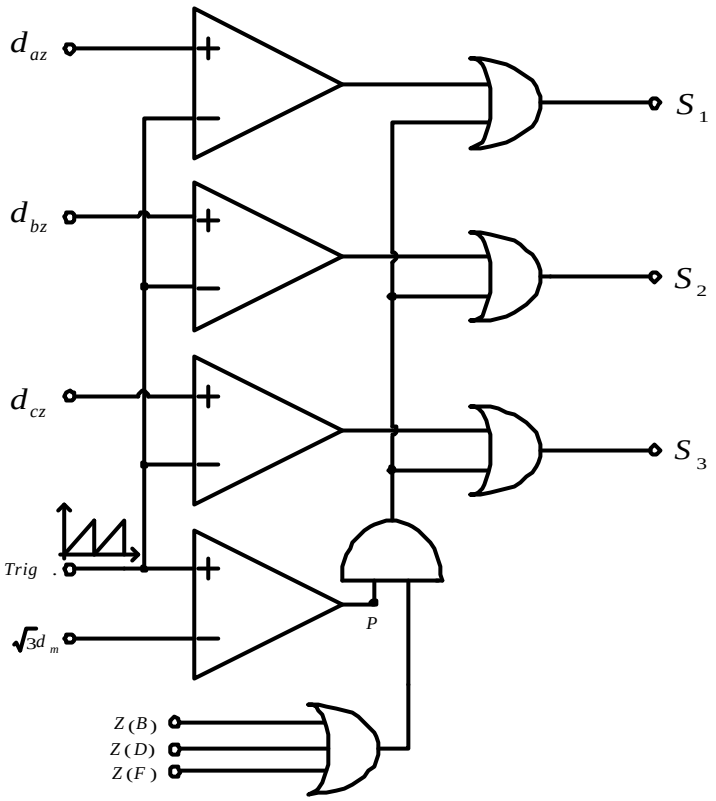

(a)

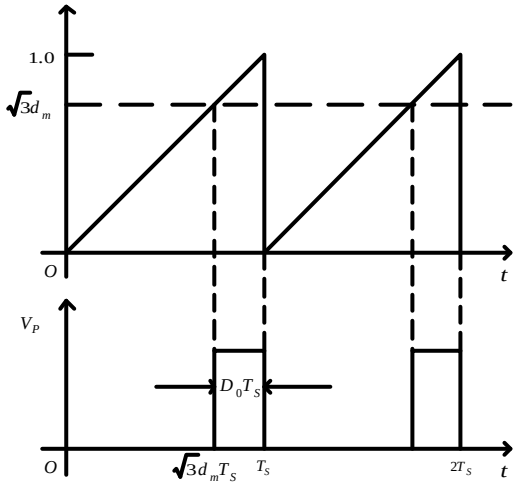

(b)

Fig. 5.3 An implementation block diagram of first switch signal generator: (a) Generating signal of S_1, S_2 and S_3, (b) Illustration of how to generate D_0T_S at the proper position for S_1, S_2 and S_3

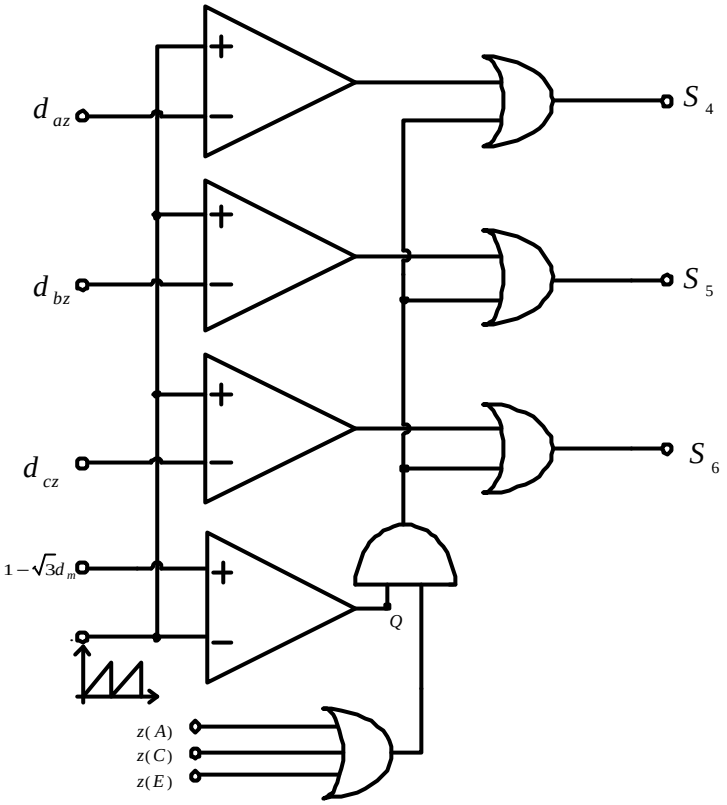

(a)

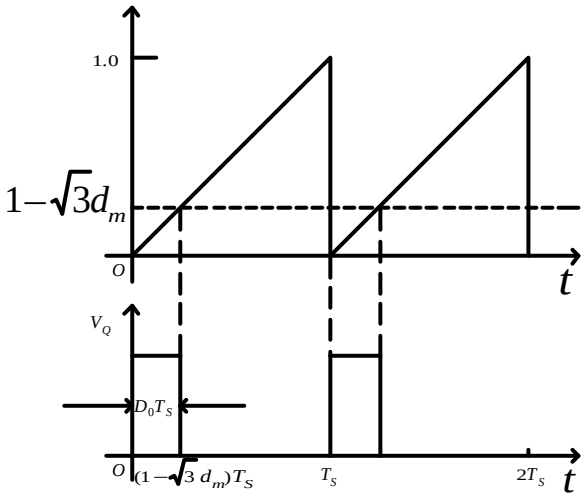

(b)

Fig. 5.4 An implementation block diagram of second switch signal generator: (a) Generating signal of S_4, S_5 and S_6, (b) Illustration of how to generate D_0T_S at the proper position for S_4, S_5 and S_6

can be observed from Fig. 5.5. Finally, from Fig. 5.5 one can see v_C is obtained by dividing V_o by D_0 to obviate the application of a v_C sensor.

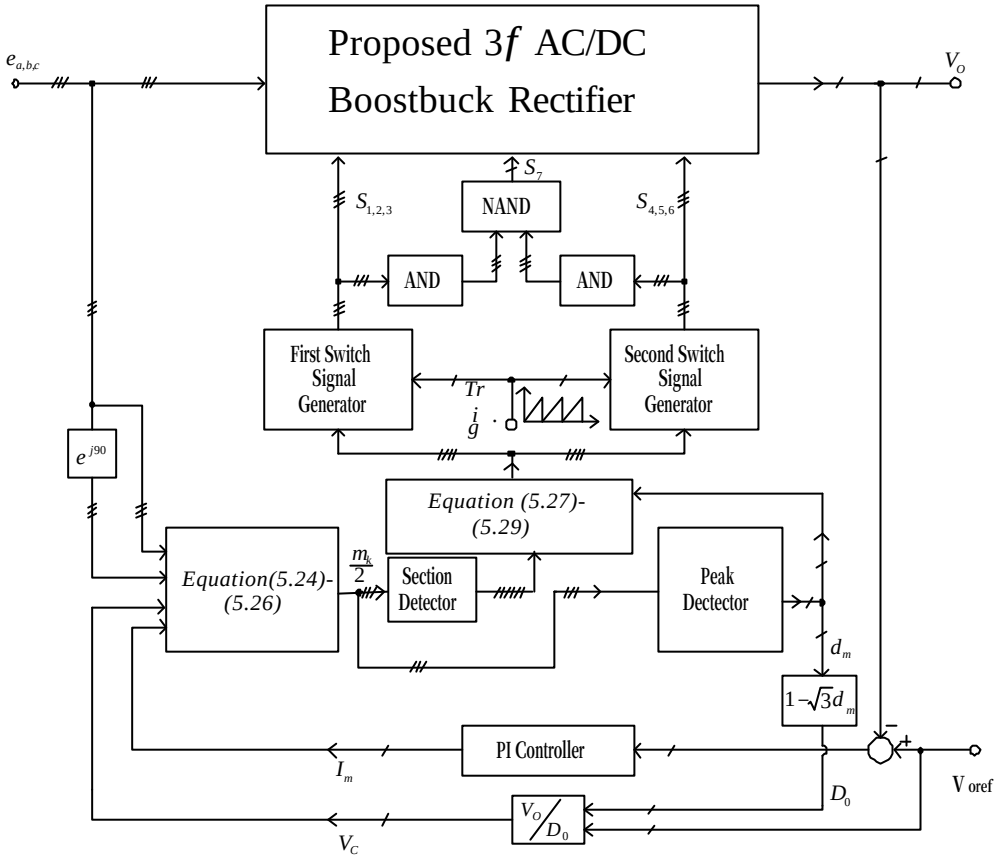

Fig. 5.5 An implementation block diagram for the proposed controller

5.4 Some Simulation results

To facilitate the understanding of the above theoretical results, some simulation results are given below as illustrations. The parameters of the converter in Fig. 3.1 are listed below for reference.

$$L_S = L = 7.5\ mH,\ \ C = C_o = 2200mF,\ R_S = 0.45\Omega,$$

Output power $\frac{V_o^{\,2}}{R} = 4\,kW$, AC line frequency 60 Hz,

Phase voltage amplitude $\frac{220\sqrt{2}}{\sqrt{3}}$ volts, Power factor = 1.0, $f_s = 3\,kHz$.

First, consider the step-down case with $V_O = 48\,V$ and $P_O = 4\,kW$. Fig. 5.6 shows the waveforms of $e_a(t)$, $5i_a(t)$, $v_O(t)$ and $v_C(t)$, respectively. From Fig. 5.6 one can see that the input AC line current is clean sinusoidal and with $pf = 1.0$. Also, the output voltage is constant and so is V_C with $V_C - V_O = 308.5\,V$. For comparison, Fig. 5.7 shows the corresponding duty ratio functions of the seven active switches. It is seen that $D_0 = 0.1346$, $V_C = 356.5\,V$ as compared with $D_0 = 0.1151$ and $V_C = 416.9\,V$ for the control strategy of the previous chapter.

Next consider the step-up case with $V_O = 500\,V$ and $P_O = 4\,kW$. Fig. 5.8 shows the corresponding simulation results, namely (a) $e_a(t)$ and $5i_a(t)$ (b) $v_O(t)$ (c) $v_C(t)$. From Fig. 5.8 one can see that $V_C - V_O$ still remains at the same, namely $\sqrt{3}V_{base} = 308.5\,V$ instead of $2V_{base}$ for the control strategy of the previous chapter. Also as a comparison, Fig. 5.9 also shows the gating signals of the seven active switches for $V_O = 500\,V$ case. It is seen that $D_0 = 0.6184$ and $V_C = 808.5\,V$ for the dead-band case as compared with $D_0 = 0.5754$ and $V_C = 868.9\,V$ for the control strategy of the previous chapter.

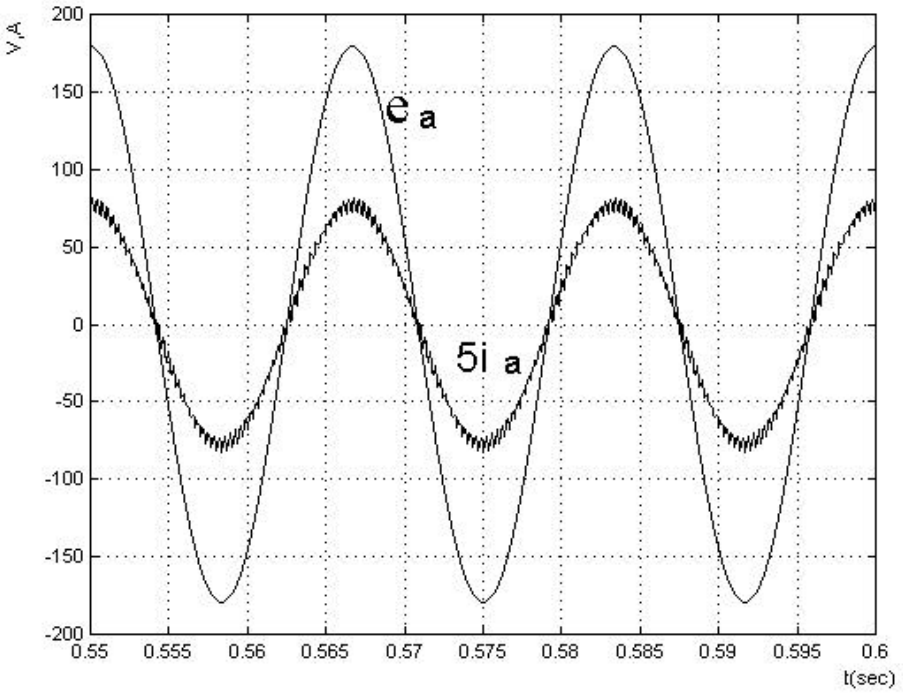
V,A
200
150
100
50
0
-50
-100
-150
-200
e a
5i a
0.55
0.555
0.56
0.565
0.57
0.575
0.58
0.585
0.59
0.595
0.6
t(sec)

(a)

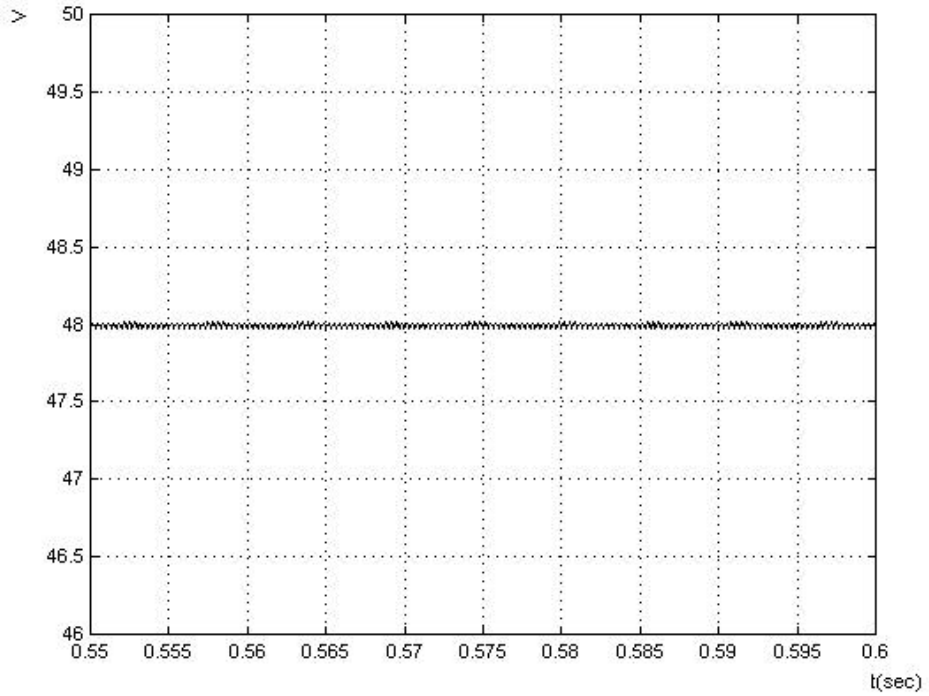
V
50
49.5
49
48.5
48
47.5
47
46.5
46
0.55
0.555
0.56
0.565
0.57
0.575
0.58
0.585
0.59
0.595
0.6
t(sec)

(b)

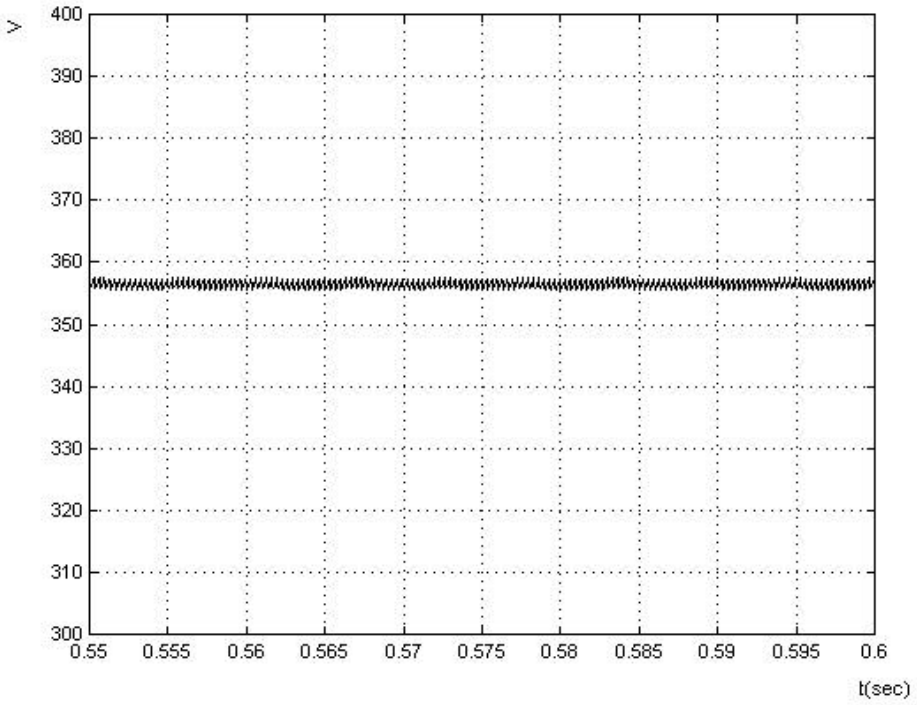

(c)

Fig. 5.6 Waveforms of (a) $e_a(t)$ and $5i_a(t)$, (b) $v_O(t)$, (c) $v_C(t)$ under step down operation

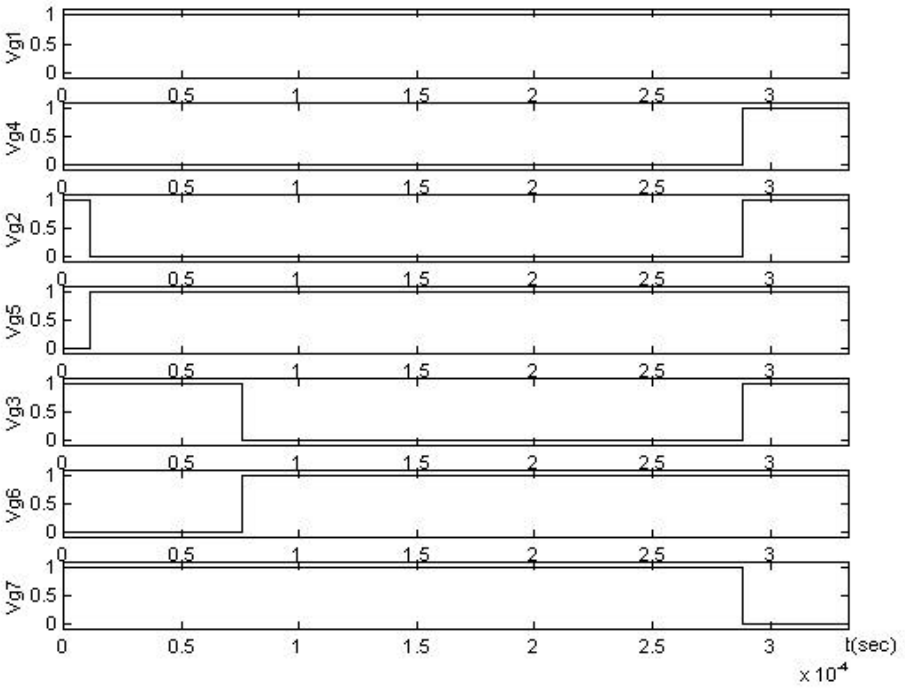

Fig. 5.7 Gating signals of the seven active switches under dead-band control

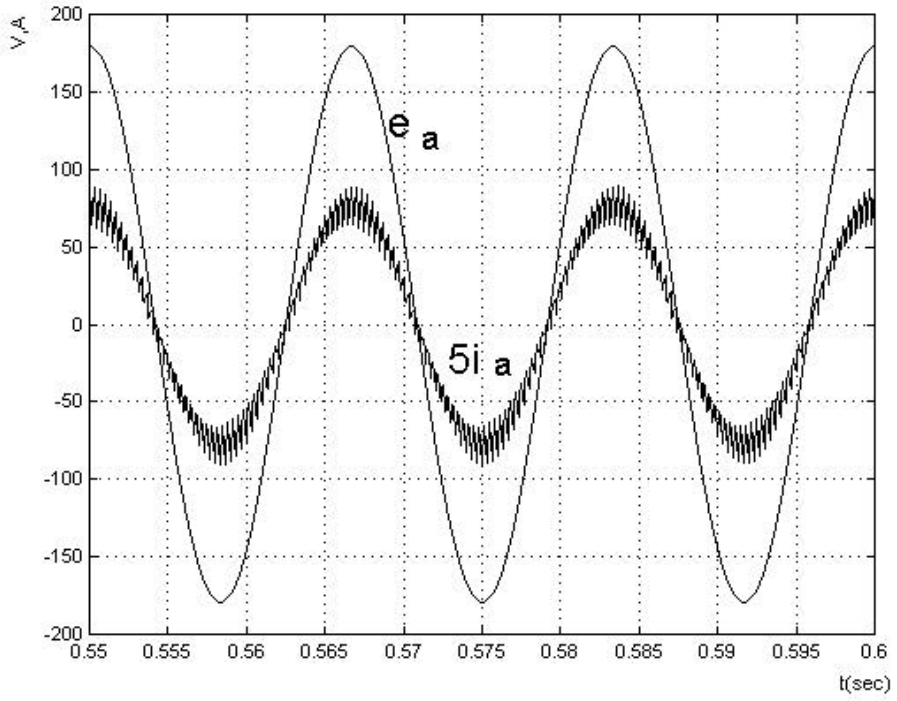
V,A
200
150
100
50
0
-50
-100
-150
-200
e a
5i a
0.55
0.555
0.56
0.565
0.57
0.575
0.58
0.585
0.59
0.595
0.6
t(sec)

(a)

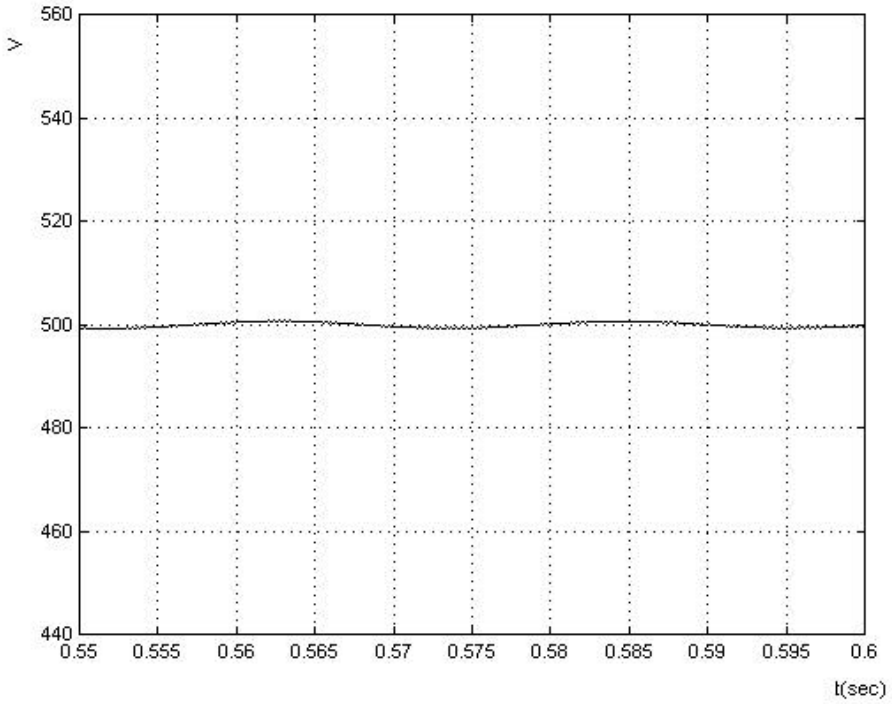
V
560
540
520
500
480
460
440
0.55
0.555
0.56
0.565
0.57
0.575
0.58
0.585
0.59
0.595
0.6
t(sec)

(b)

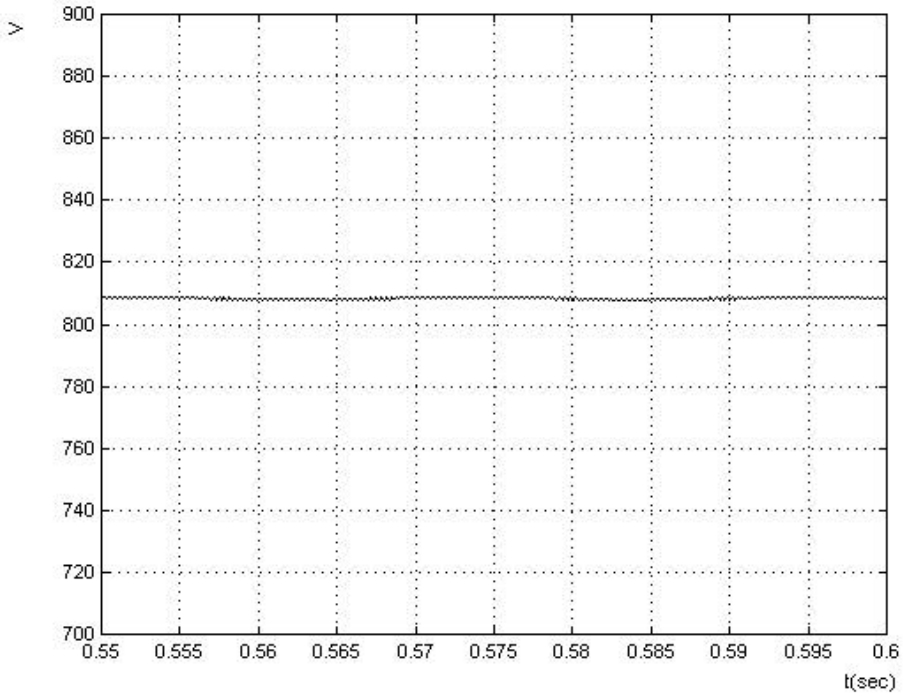

(c)

Fig. 5.8 Simulation waveforms of the step up case (a) $e_a(t)$ and $5i_a(t)$, (b) $v_O(t)$, (c) $v_C(t)$

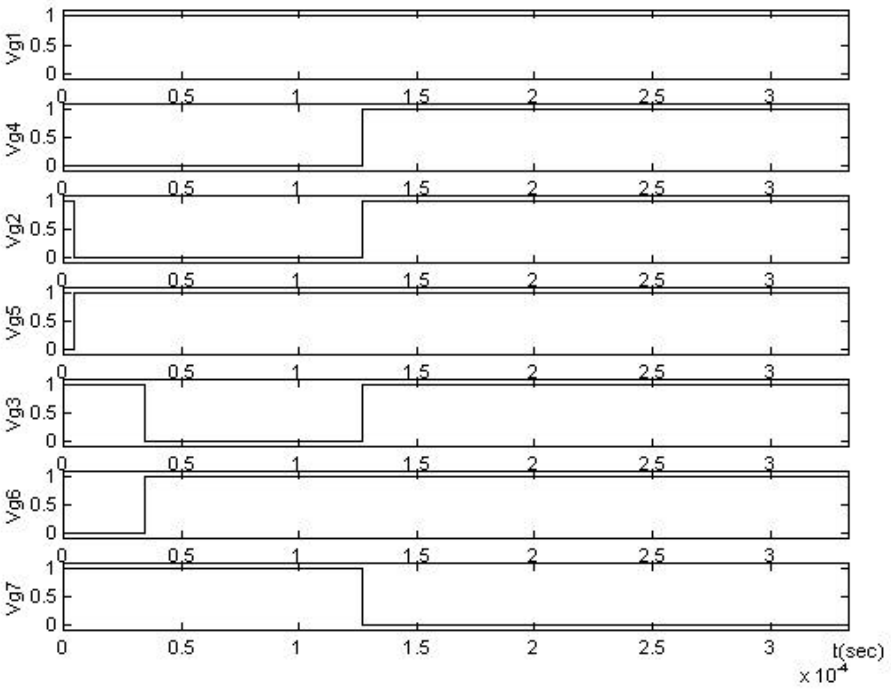

Fig. 5.9 Gating signals of the seven active switches for $V_O = 500\,V$ and $P_O = 4\,kW$

Third, consider the regeneration cases. Again, the simulation condition is the same as used in the previous chapter, namely by applying a DC voltage source in series with a resistor to the output through a switch and under close loop control. Fig. 5.10 shows the simulation results of $e_a(t)$, $5i_a(t)$, $v_O(t)$ and the corresponding gating signals with $V_O = 48\,V$. Similarly, Fig. 5.11 shows the simulation results for $V_O = 500\,V$ case. Again, the 180^0 phase difference between e_a and i_a shows the regeneration mode correctly. Also, $V_C - V_O$ remains a constant, namely 329.84 V for P_O=4kW.

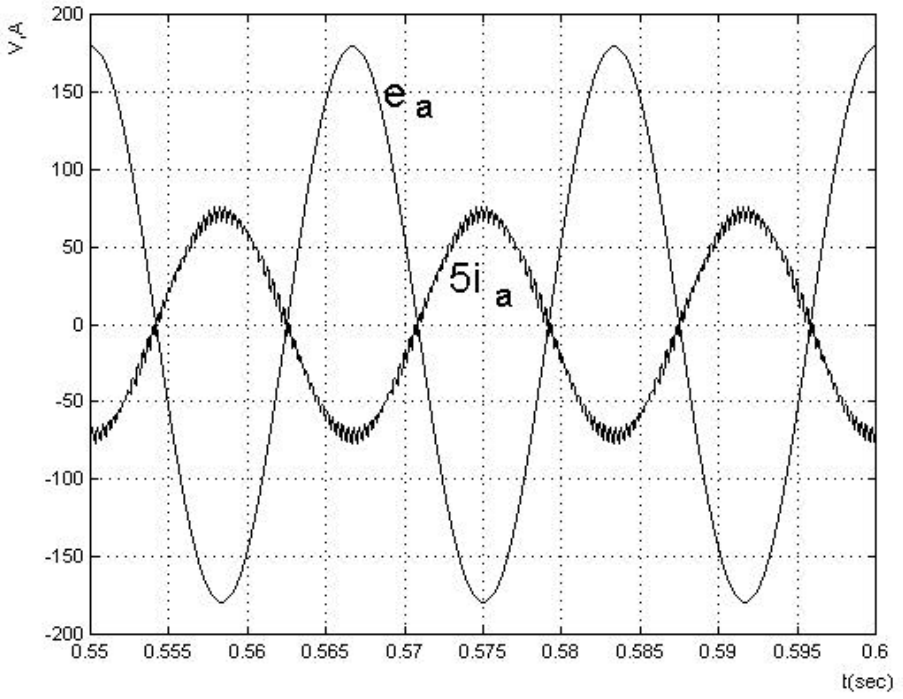

(a)

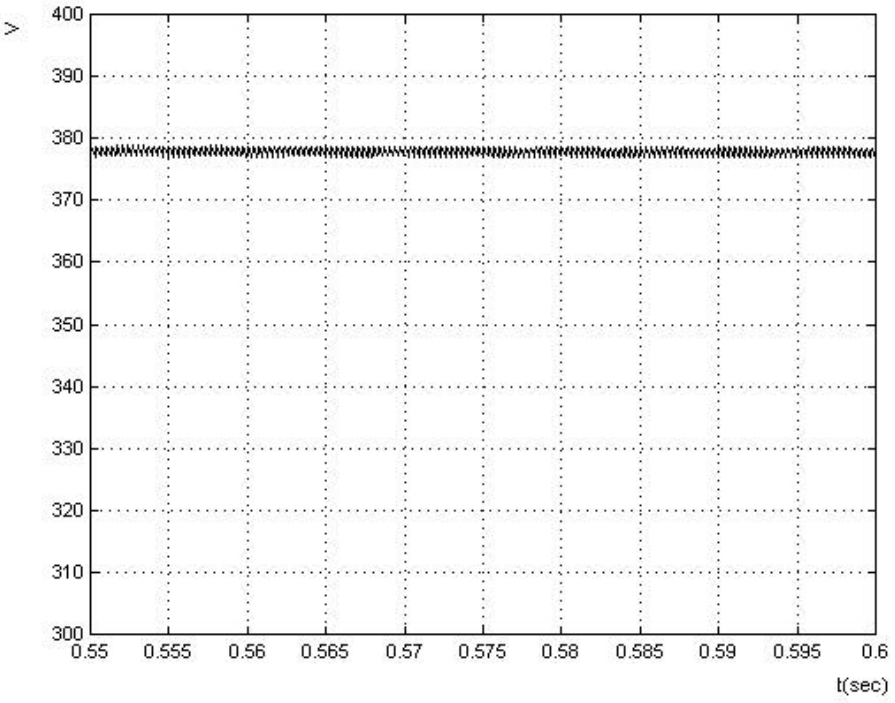

(b)

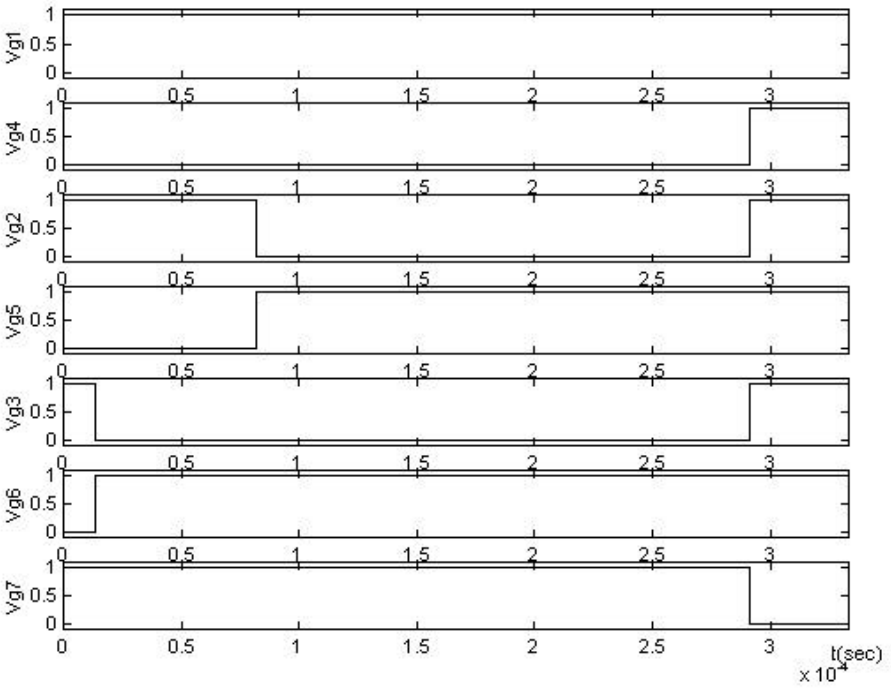

(c)

Fig. 5.10 Simulation waveforms for step down case $V_O = 48\,V$: (a) $e_a(t)$ and $5i_a(t)$, (b) $v_C(t)$, (c) gating signals of seven active switches under regeneration mode

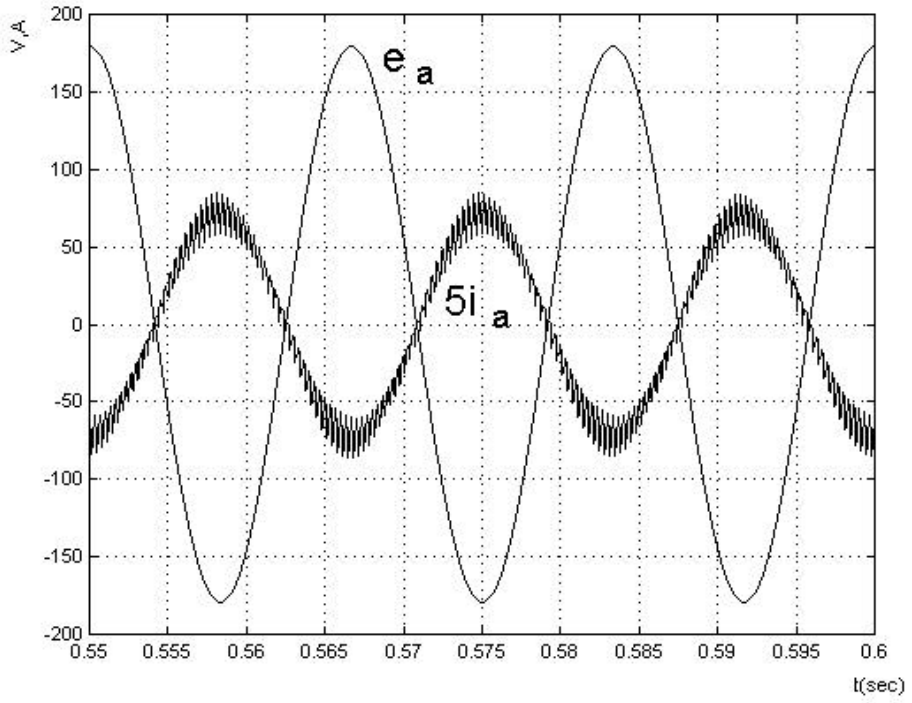
V,A
200
150
100
50
0
-50
-100
-150
-200
e a
5i a
0.55
0.555
0.56
0.565
0.57
0.575
0.58
0.585
0.59
0.595
0.6
t(sec)

(a)

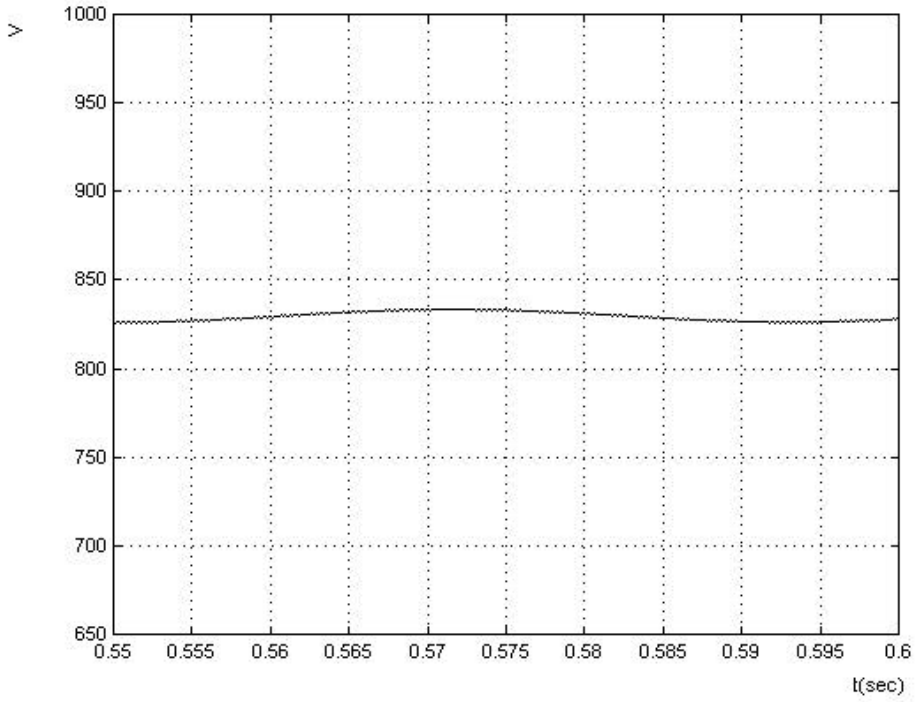
V
1000
950
900
850
800
750
700
650
0.55
0.555
0.56
0.565
0.57
0.575
0.58
0.585
0.59
0.595
0.6
t(sec)

(b)

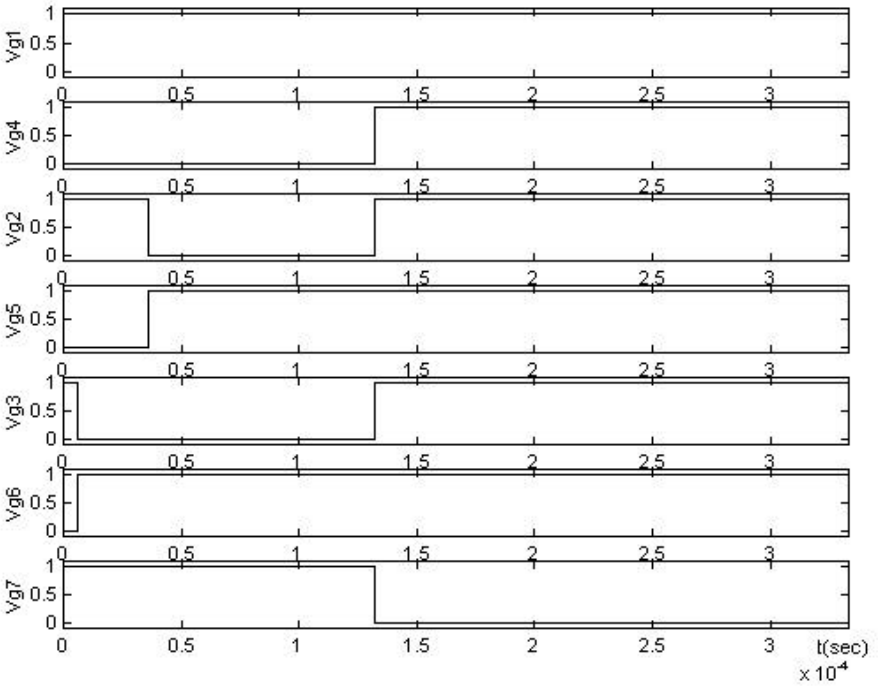

(c)

Fig. 5.11 Simulation waveforms for step up case $V_O = 500\,V$: (a) $e_a(t)$ and $5i_a(t)$, (b) $v_C(t)$, (c) gating signals of seven active switches under regeneration mode

Fourth, Fig. 5.12 also shows the switching numbers of one active switch for the dead-band control strategy. For comparison, the switch number of one active switch for the maximum constant D_0 control strategy of chapter four is also plotted on the same figure. From Fig. 5.12 one can clearly see the reduction of the switching number is about one sixth for each switch, S_k, k=1, 2, …6. Certainly, the switching loss reduction can also be expected for the dead-band control strategy.

Finally, to have a better insight about the characteristic of the dead-band control strategy, Fig. 5.13 shows the duty ratio functions of $d_1(t)$ for (a) $V_O = 48\,V$,

rectifier mode, (b) $V_O = 500\,V$, rectifier mode, (c) $V_O = 48\,V$, regeneration mode (d) $V_O = 500\,V$, regeneration mode for $P_O = 4\,kW$. It is interesting to see from Fig. 5.13 that the resulting duty ratio functions remain continuous. This is because maximum D_0 has been adopted in the control strategy. Otherwise, the corresponding duty ratio functions will become discontinuous.

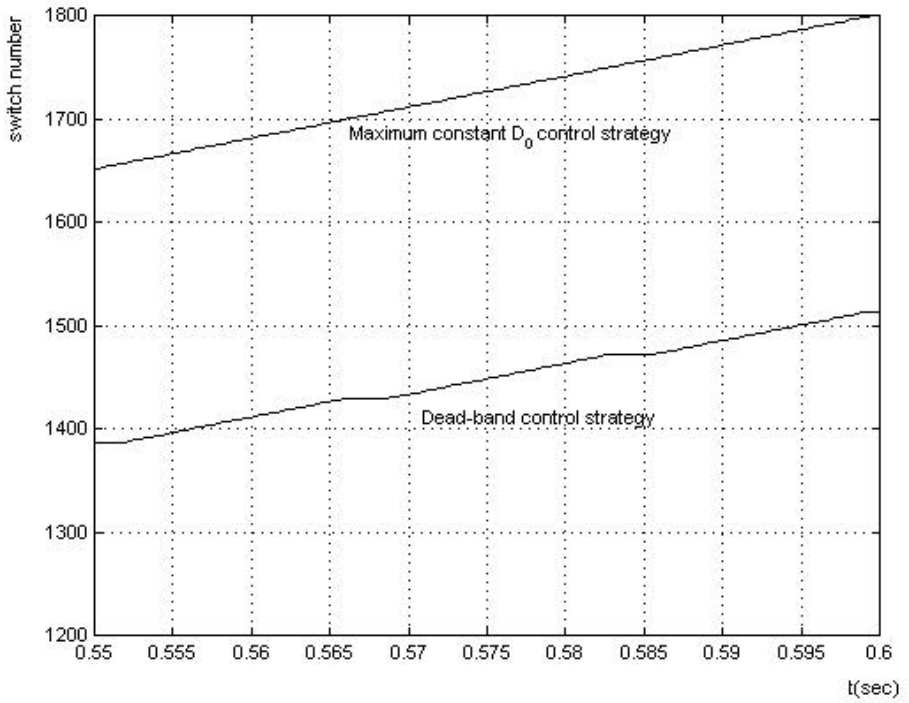

Fig. 5.12 Comparison of switching number of one active switch

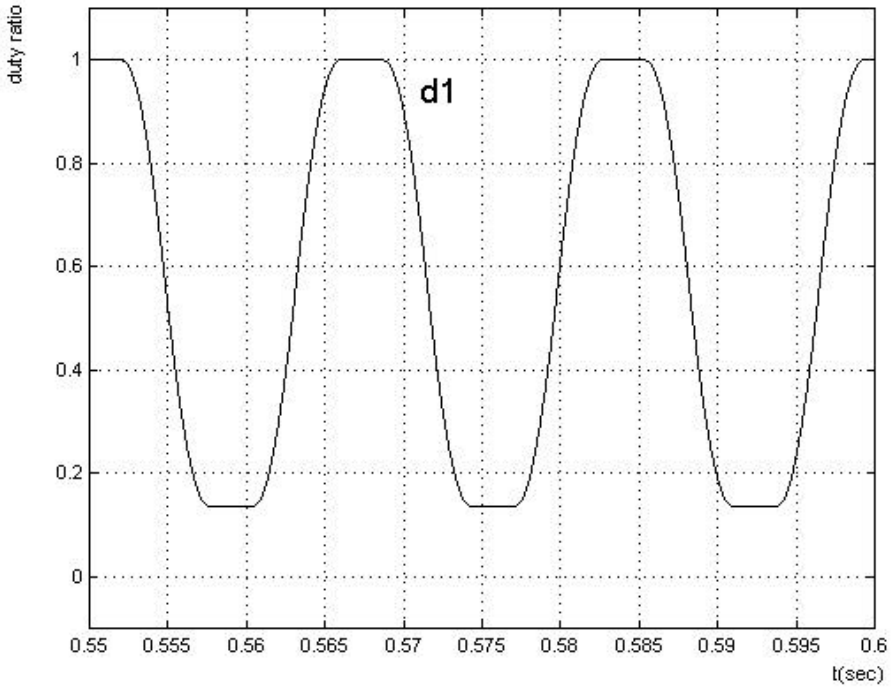
duty ratio
d1
1
0.8
0.6
0.4
0.2
0
0.55
0.555
0.56
0.565
0.57
0.575
0.58
0.585
0.59
0.595
0.6
t(sec)

(a)

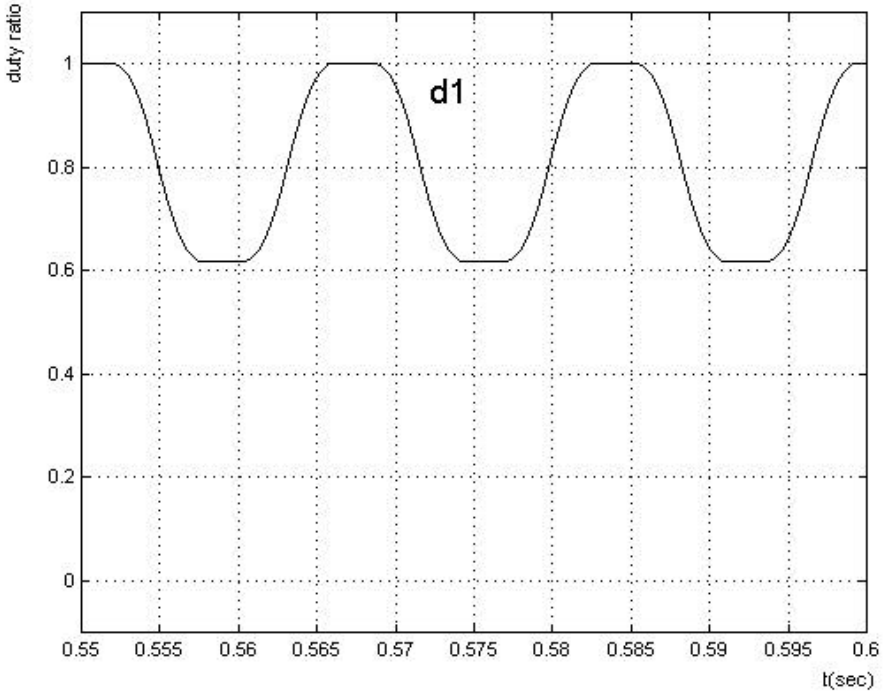
duty ratio
d1
1
0.8
0.6
0.4
0.2
0
0.55
0.555
0.56
0.565
0.57
0.575
0.58
0.585
0.59
0.595
0.6
t(sec)

(b)

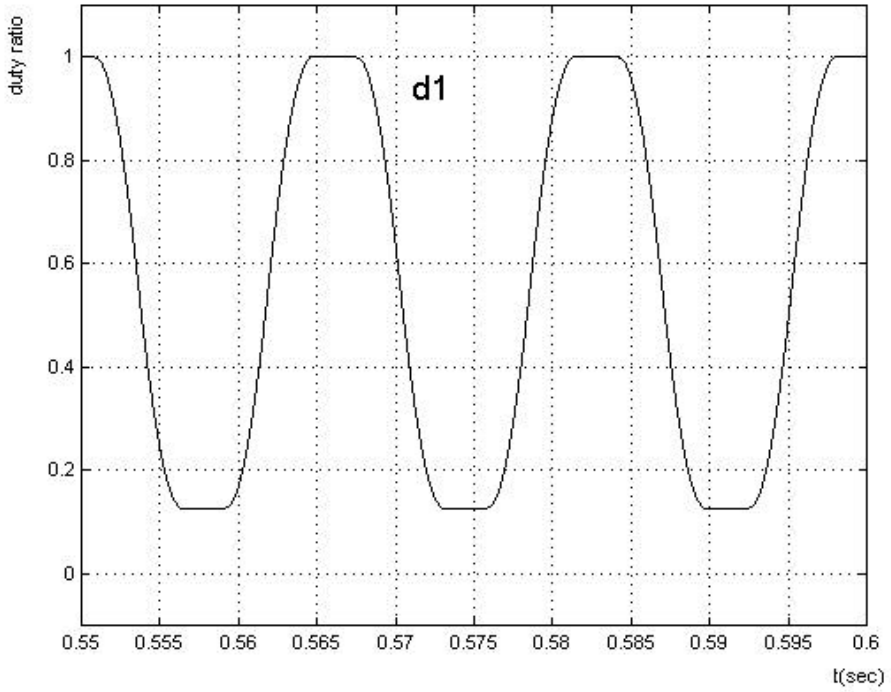

(c)

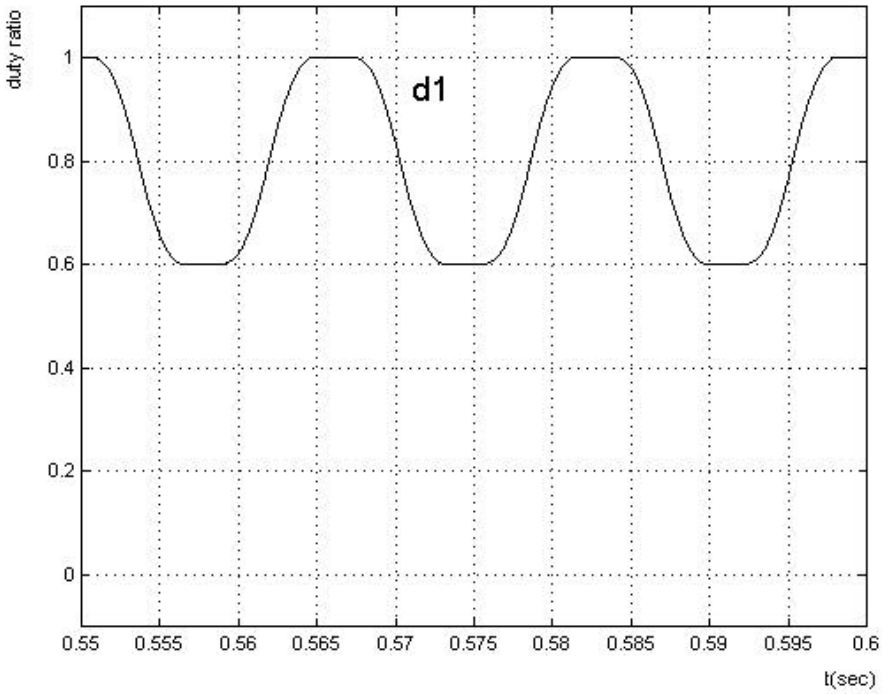

(d)

Fig. 5.13 Duty ratio function of S_1: (a) $V_O = 48\,V$, rectifier mode, (b) $V_O = 500\,V$, rectifier mode, (c) $V_O = 48\,V$, regeneration mode, (d) $V_O = 500\,V$, regeneration mode